TECTONICS, VOL. 17, NO. 6, PAGES 955-972, DECEMBER 1998

Mechanical modeling of compressional basins: Origin and interaction of faults, erosion, and subsidence in the Ventura basin, California

Fernando Niño [1]
Laboratoire de Géophysique et Tectonique, CNRS, Université Montpellier II, Montpellier, France
Bureau de Recherches Géologiques et Minières, Marseille, France

Jean Chéry
Laboratoire de Géophysique et Tectonique, CNRS, Université Montpellier II, Montpellier, France

Jean-Pierre Gratier
Laboratoire de Géophysique Interne et Tectonophysique, CNRS-Observatoire, Université Joseph Fourier
Grenoble, France

Abstract. Using geophysical observations and some basic geological ideas on the present structure of the Ventura basin, we model its possible mechanical evolution during the last 4 million years. We use a two-dimensional finite element model with frictional and elastoviscoplastic rheologies that allow strain localization. This allows us to study the mechanical origin of the San Cayetano thrust fault (SCF) and its interaction with the Oak Ridge fault (ORF). The results of our modeling indicate that the geometry and activity of a shear zone which mimics the San Cayetano fault are conditioned both by the preexistence of the Oak Ridge fault and by the shape of the brittle-ductile transition. Furthermore, the presence of a décollement level is shown to favor the development of the San Cayetano fault shear zone as a low-angle structure. The value of the effective friction on the Oak Ridge fault is evaluated from this model. Possible values of the viscosity of the sediments are also estimated; it is shown that low sediment viscosity may completely hinder the activity of such a fault at the surface, while slip at depth continues. The stratigraphic profile of the basin is also shown to depend on the relative strengths of the ORF and SCF, which also provide an explanation for the shortening and rapid subsidence of the basin.

1. Introduction

Tectonic phenomena are the consequence of the complex interaction of a large number of factors, including the state of stress, crustal geometry, rheology, fault activity, erosion and sedimentation. The temporal evolution of such a geodynamical system can be calculated in the framework of continuum mechanics, and it can be used to study the simultaneous effects of many geological processes. Mechanical modeling is thus a useful tool for gaining insights into the physical behavior of complex geodynamical systems, using available data as the main constraints on the inputs and results of the models.

The development of compressional basins is a good example of such complex interactions, and the Ventura compressional basin is used here to show how numerical modeling may help us understand the development and interaction of complex structures. As the Ventura basin is a zone of high potential seismic hazard, this approach may also prove useful by giving a better view of recent crustal deformation in this area.

The Ventura basin, in the Transverse Ranges (southern California), is a particularly well-studied zone that has undergone tectonic inversion (a compressional phase which follows an extensional one) and which shows the development of a compressional basin bounded by thrusts with opposite dips. Extensive geological studies have been carried out in this zone, giving an accurate idea of present-day subsurface geometry (to a depth of ~5 km). Seismic, geodetic, and geochronological data give further information on structure, stratigraphy, and deformation rates. As in many inverted basins, structures created throughout the extensional phase have an important influence on the behavior of the tectonic system during transpression [*Butler*, 1989]. Forward modeling of the evolution of the Ventura basin is thus useful for asserting some basic mechanical properties of this tectonic system and for constraining the geometry of faults at depth. We undertook a parametrical study of the coupled effects of erosion, fault strength, and the presence of a décollement during the compressional phase of the Ventura basin (last 4 m.y.), and we compared its results with present-day fault surface geometry, topography, and stratigraphy to reconstruct the tectonic history. The present study attempts to explain two interesting processes: (1) the forma-

[1] Now at: Department of Geology and Geophysics, University of Edinburgh, Edinburgh, United Kingdom.

Paper number 1998TC900007.
0278-7407/98/1998TC900007$12.00

tion of the San Cayetano fault, and (2) the subsidence of the basin bounded by the Oak Ridge and San Cayetano faults. After a brief presentation of the tectonic setting of the Ventura basin, we present an historic reconstruction of the recent deformation in this basin in order to determine the general assumptions of the model for the geometry of the early structure, for the kinematics of the deformation, and for the boundary conditions. Then we establish the principles of the numerical method and the rheological model used, before presenting and discussing the results.

2. Tectonic History: The Kinematic Constraint

The Ventura basin (Figure 1) is bounded to the north by the San Cayetano fault and to the south by the Oak Ridge fault. The 1971 San Fernando (Mw=6.6), the 1994 Northridge (Mw=6.7), and some other earthquakes have been associated with thrust faults within this basin or with their eastern prolongations [*Yeats and Huftile*, 1995; *Davis and Namson*, 1994]. Because of the importance of accurately establishing earthquake hazards in the region, the entire Los Angeles area has been extensively studied, and particularly the Los Angeles and Ventura basins [*Hauksson*, 1990; *Shaw and Suppe*, 1996; *Yeats et al.*, 1994]. The Ventura basin was formed by large-scale crustal extension in the late Oligocene; subsequent tectonic movements have created a clockwise rotation of the western Transverse Ranges block of more than 90° [*Luyendyk et al.*, 1980; *Crouch and Suppe*, 1993; *Nicholson et al.*, 1994]. About 6 m.y. ago, sedimentation and subsidence rates in the basin were such that the Miocene-Pliocene sequence now observed is one of the thickest in the world [*Yeats*, 1978], making it an interesting case for basin subsidence modeling. The present-day compressive regime began 3-4 m.y. ago as the area experienced uplift, active faulting, and folding [*Molnar*, 1992]. However, stress in the Ventura basin since Pliocene times has remained approximately constant in direction (NNE) and perpendicular to the basin axis, as deduced from fold axes [*Yeats et al.*, 1994; *Gratier*, 1995] and the thread geometry of the San Cayetano fault [*Thibaut et al.*, 1996]. Consequently, the last 4 m.y. of tectonic history of the Ventura basin can be modeled, to a first approximation, as a two-dimensional process on a vertical cross section.

2.1. Preexisting Faults

The Oak Ridge is assumed to be a reactivated Miocene normal fault, possibly a ring fault with northward curvature related to emplacement of a large volcanic caldera in the western Santa Monica Mountain [*Yeats*, 1987a; *Yeats and Huftile*, 1995]. Evidence that the Oak Ridge fault was active as a normal fault during Miocene time is found in the field [*Yeats*, 1987b]. *Yeats et al.* [1994] proposed a west dipping Oak Ridge normal fault during Miocene times, which was subsequently rotated clockwise. However, neither the exact location of this fault nor the evolution of its dip during the rotation is known. The dip of the Oak Ridge fault is presently toward the south (between 60° and 80°, as in Figure 1b, although in some localities, dips outside this range are observed), as is confirmed by well data to a depth of several kilometers. The possible inversion of the dip direction during the initial stages of compression, or the crosscutting of a preexisting normal fault by a thrust fault [*Huftile and Yeats*, 1996] is difficult to reconstruct, and we did not try to model this early evolution. Following the model proposed by *Huftile and Yeats* [1996, in their Figure 3], we started the modeling process with the Oak Ridge fault dipping toward the south, as it does at present. The recent earthquake [*Yeats and Huftile*, 1995] on the Northridge south dipping fault, presumed to be part of the Oak Ridge system, attests to the large lateral extent of the south dipping structure (aftershocks image the fault up to 20 km of depth) and justifies our choice of a preexisting south dipping Oak Ridge fault for the first step of the modeling of the N-S compression (Figure 2).

The San Cayetano thrust fault is rather different from the Oak Ridge fault. The average northward dip is lower (about 40°), and stratigraphic relations indicate that thrust displacement occurred on previously folded structures [*Huftile and Yeats*, 1996, Figure 3]. It appears then that the development of the San Cayetano fault may have been related to the early thrust movement on the south dipping Oak Ridge fault, one of the ideas motivating the present study.

2.2. Stratigraphy and Folding

The stratigraphic composition of the cross section in Figure 2 is well constrained to a depth of 5 km, since a number of exploration wells have been drilled in the basin (a full description of stratigraphy was made by *Yeats et al.* [1994]). The main stratigraphic features in which we are interested are simple, and we describe them briefly. South of the Oak Ridge fault the basement is overlain by Eocene and Paleocene series, where almost no deformation is observed. North of the Oak Ridge fault, 1 m.y. ago, the basement under the basin and that beneath the block north of the San Cayetano fault were at the same level, overlain by the Modelo formation (Figure 2c) [*Huftile and Yeats*, 1996]. However, at that time the sedimentary cover north of the Oak Ridge fault was probably already deformed as attested by large folds, which developed prior to the formation of the San Cayetano fault; this is seen in the reconstruction of cross section AA' (near the Topatopa mountains in Figures 1b, 2b, and 2c) [*Huftile and Yeats*, 1996]. Such early folds are also present on cross section BB' (west of AA', Figure 1), but they were not cut at the same level by the San Cayetano fault, probably because this fault is oriented obliquely, relative to these early structures. The folded sedimentary sequence is found to be a succession of alternating shales and sandstones and is therefore relatively weak. It is calculated to be ~7 km thick [*Huftile and Yeats*, 1996].

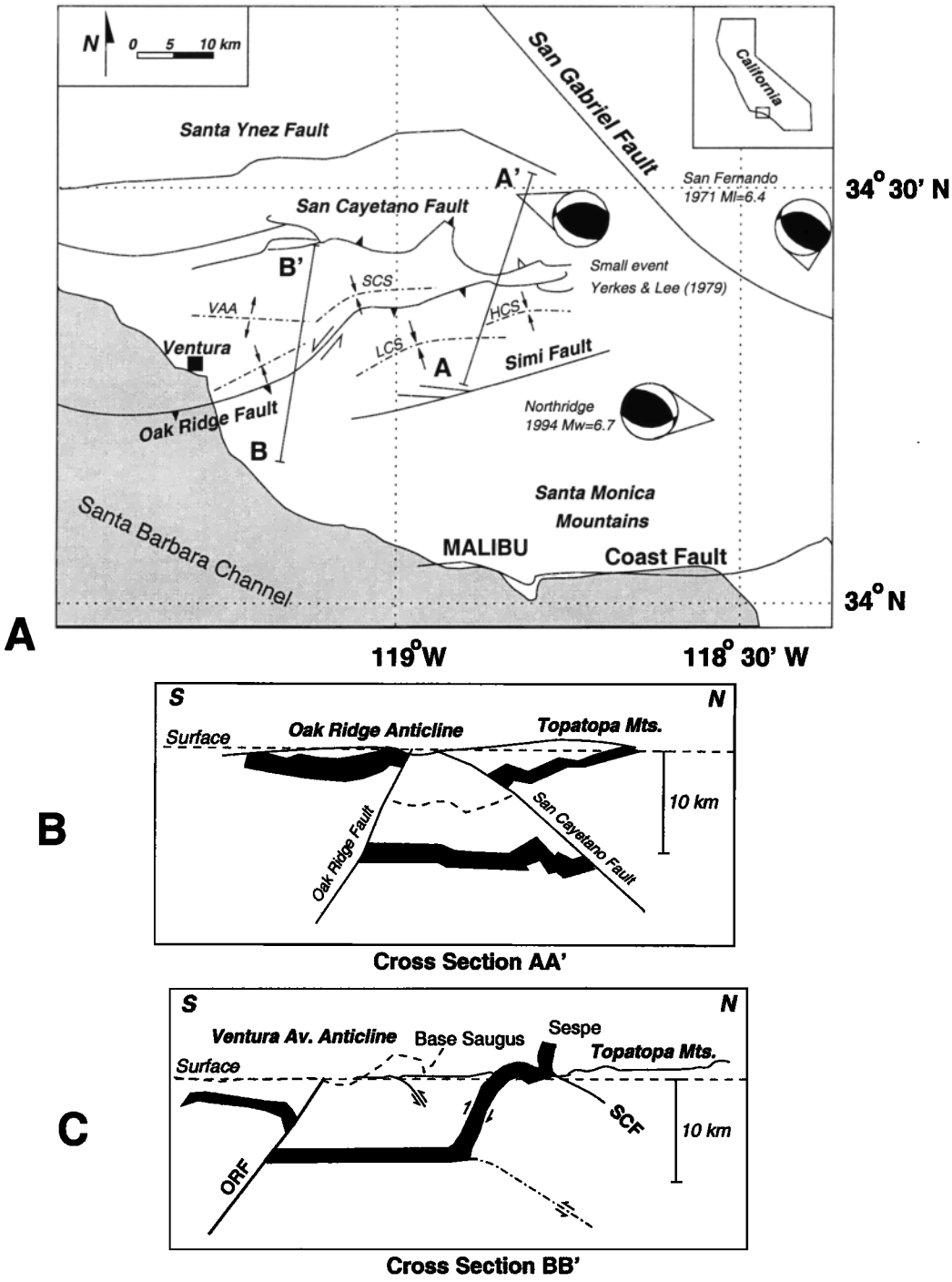

Figure 1. (a) Map view of southern California showing the location of cross sections AA' and BB' (modified from *Huftile and Yeats* [1996], ©1996 Seismological Society of America. All rights reserved). Focal mechanisms for three earthquakes in the zone are also plotted, including a small one north of the San Cayetano fault [*Yerkes and Lee*, 1979]. Four fold axes have also been included: HCS, Happy Camp Syncline; LCS, Long Canyon Syncline; SCS, Santa Clara Syncline; VAA, Ventura Avenue Anticline. (b) Schematic cross section showing the present day geometry of the Ventura basin along profile AA' (modified from *Huftile and Yeats* [1996]). The black stratigraphic marker is the Sespe formation. The dotted line indicates the base of the Pleistocene Saugus formation, whose dating has provided the main constraints for the tectonic history of the basin (see legend of Figure 2). This sequence is ~4 km thick in the footwalls of the Oak Ridge and San Cayetano faults. (c) Schematic cross section along profile BB', west of profile AA'; the blind thrust shown and the prolongation of the San Cayetano fault can be interpreted as consequence of a décollement at depth (see section 4.1.4; modified from Figure 3 of *Huftile and Yeats* [1995]). SCF, San Cayetano thrust fault; ORF, Oak Ridge fault.

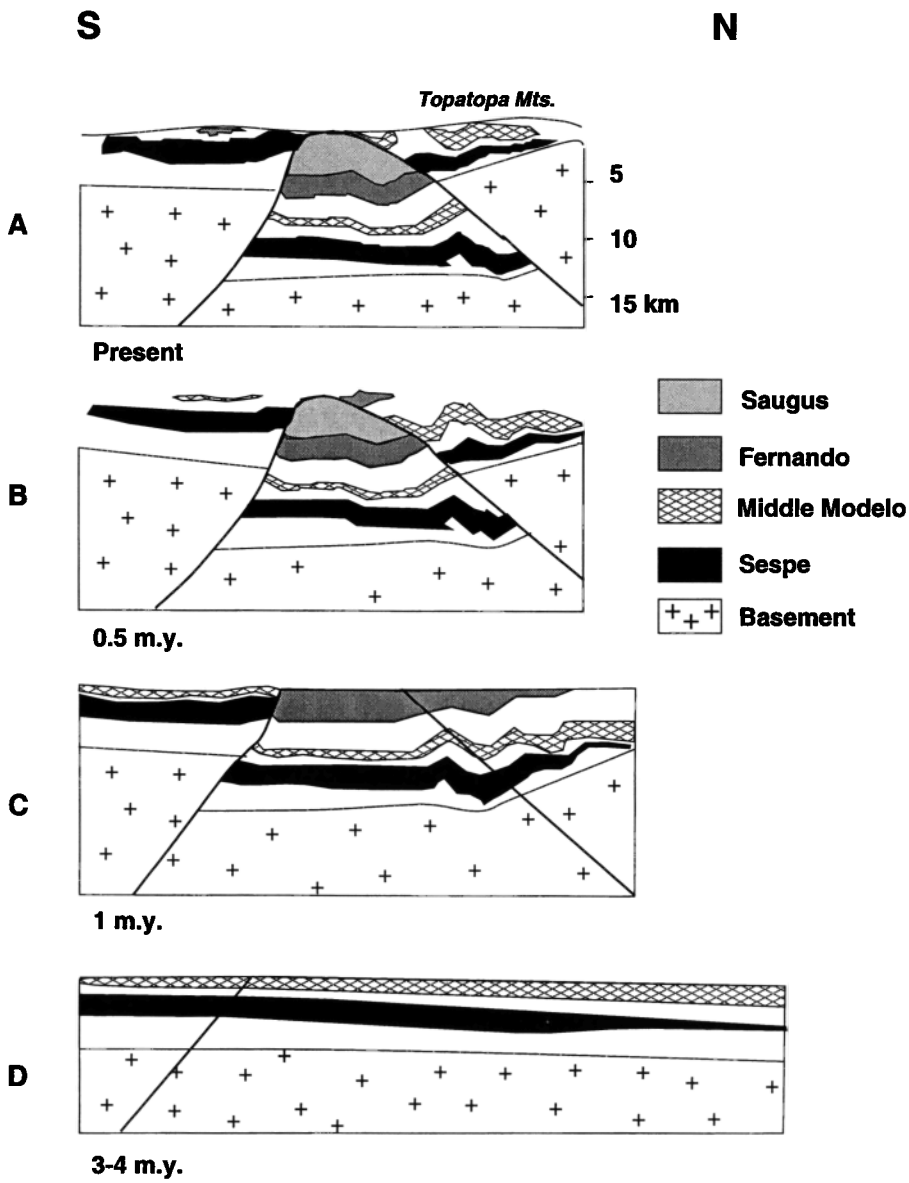

Figure 2. Schematic evolution of the east central Ventura basin along profile AA' of Figure 1 for (a) preent, (b) 0.5 m.y., (c) 1 m.y., and (d) 3-4 m.y. (simplified after *Huftile and Yeats* [1996]). The San Cayetano fault appears between 3-4 and 1 m.y. ago (steps $d \Rightarrow c$); this deformation phase is modeled with the continuum approach for strain localization. The phase of basin subsidence (steps $c \Rightarrow a$) is modeled assuming that both the Oak Ridge and San Cayetano faults are frictional surfaces (with Coulomb's law for friction). The Saugus formation varies upward from shallow marine to nonmarine strata, and it has been dated to 975 ± 75 thousand years. The Fernando formation is of Pliocene age. The middle Modelo formation was deposited in a middle-late Miocene and comprises shales and sandstones. The Sespe formation is a nonmarine Eocene-Oligocene sequence.

2.3. Deformation Rates

Geodetic velocities throughout the Ventura basin have an important spatial variation; however, measurements made by various authors of the N-S shortening rates are consistent: 4.6-7 mm/yr [*Feigl et al.*, 1993] and 5-8 mm/yr [*Larsen et al.*, 1993; *Donnellan et al.*, 1993]. Contraction rates estimated from geological observations are highly variable since they depend largely on the uncertainty, on the age of the formations, and on the duration of the N-S compression phase [*Molnar*, 1992]. Recent determinations of shortening rates through the Ventura basin using geological observations are more and more consistent: 6 mm/yr [*Gratier*, 1995] and 5.8-10.6 mm/yr [*Huftile and Yeats*, 1996], which also agree with estimates based on available Global Positioning System data. For simplicity, we will assume a constant shortening rate of 1 cm/yr for the Ventura basin.

3. Mechanical Modeling: Principles and Parameters

3.1. Fault Modeling : Continuum and Frictional Approaches

Faulting in the Earth's crust can be understood as the expression of brittle fracture of rock on a large scale. In the laboratory, large-scale deformation of solids is rarely attained homogeneously; more often than not, deformation becomes intensely concentrated in a narrow zone where fractures finally develop (this may result from stress concentrations, inhomogeneities, or any other physical mechanism that greatly reduces the strength of the material). Consequently, rather than studying the very complex process of dynamic brittle fracture of solids, faulting can be represented by mechanisms of strain localization in continua, provided mesh dependency problems are suitably addressed. The framework within which this phenomenon of strain localization can be understood has been established for solids obeying a certain kind of elastic-plastic constitutive law [*Rudnicki and Rice*, 1975], and it treats strain localization as a discontinuity in strain rate [*Ode*, 1960]. With this approach we can study the mechanical parameters that condition the origin of the San Cayetano fault. However, preexisting faults need not be modeled as zones of plastic weakness and can be treated more simply as surfaces with frictional properties. In this case, slip along these surfaces will be governed by Coulomb's friction law, using the nonsmooth contact dynamic method [*Jean and Touzot*, 1988; *Jean and Moreau*, 1991].

3.2. Finite Element Method Analysis

Modeling of geodynamical processes in two dimensions is done by using a finite element code in large strain under quasi-static conditions. We use a Lagrangian description of the geological medium with quadrilateral elements formed by assembling pairs of triangular elements of constant strain (this code is fully described by *Hassani* [1994]). The implementation of the dynamic relaxation technique [*Board*, 1989; *Cundall*, 1989] permits the explicit solution of the system's governing equations. An elastoplastic material following a Drucker-Prager rheology that allows strain localization [*Leroy and Ortiz*, 1989] is used to model the upper crust, while some sediments and the middle and lower crust are supposed to be linear viscous materials. Boundary conditions are imposed both as velocities (imposed horizontal shortening rate) and as a hydrostatic pressure at the base.

To ensure stability of the solution and to guarantee the fulfillment of the quasi-static assumption, a remeshing technique is applied to the system when either the overall quality of the mesh is under a certain threshold or when erosion reduces the surface of any element to half its initial value (for details, see Appendix A). Immediately after remeshing, interpolation of scalar (e.g. velocity components and eroded and sedimented masses) and tensorial quantities (stress and strain) is needed to transfer this information from the previous mesh to the new mesh. This is a purely mathematical procedure, where no physical principles are imposed. Finally, a stabilization phase permits the system to regain equilibrium while verifying stress admissibility conditions.

To avoid the phenomenon of mesh locking in our calculations of strain localization [*Nagtegaal et al.*, 1974], we use a mixed formulation technique [*Cundall*, 1989]. Our numerical experiments were done with an average number of 2500 quadrilateral elements and 200,000 time steps to ensure both stability of the solution and quasi-static conditions (the relaxation time of the viscous middle and lower crusts should also be much greater than the time step).

3.3. Crustal Rheology

The composition of the continental crust has been extensively studied, and some relatively standard models of it have been put forward [*Brace and Kohlstedt*, 1980; *Kirby*, 1983; *Carter and Tsenn*, 1987]. Depending on which deformation processes are to be modeled, the rheological behavior of the upper crust can be approximated by elastic, viscoelastic, or elastoplastic laws. Elastic behavior is extensively used to model coseismic deformation with dislocation models [*Ben-Menahem and Singh*, 1968; *Savage*, 1980; *Okada*, 1992] but is not suited to model long term geodynamic processes since elastic deformation is, by definition, reversible, and owing to the occurrence of irrealistically high stresses. In contrast, both viscous and elastoplastic rheologies can model large geological deformations. For example, linear viscoelasticity is widely used for analytically studying the mechanics of folds in geology [*Ramberg*, 1964; *Ramsay and Huber*, 1987] and is one of the rheological laws that we will adopt for studying the behavior of basin sediments. Inverse modeling on basin deflection [*Bills et al.*, 1994] showed that the upper crust may behave as a linear viscous material with viscosity between 10^{26} and 10^{18} Pa·s (0-15 km depth); we will use viscosity values close to 10^{20} Pa·s as in *Gratier and Gamond* [1990]. Elastoplasticity takes into account the qualitative change in the response of a material to deformation when strain is greater than a yield limit, the boundary between reversible and irreversible deformation. One of the simplest laws of this kind, which is dependent on both deviatoric stress and hydrostatic pressure, is Drucker-Prager's law. Its main parameters are similar to those of Mohr-Coulomb's law, namely cohesion c and the angle of internal friction, φ. We will assume a low-cohesion upper crust with a value $c = 10^5$ Pa, a Young's modulus $E = 10^{11}$ Pa, a Poisson's ratio of $\nu = 0.25$, and an angle of internal friction $\varphi = 30°$, the average values for cohesive rocks [*Jaeger and Cook*, 1976]. In our models, sediments will be considered either as being an integral part of the crust (with the same elastoplastic rheology) or as a separate (viscous) region.

The rheology of the middle and lower crusts will be as simple as possible, using linear viscosity. The standard val-

ues of linear viscosity for this part of the crust range between 10^{20} and 10^{23} Pa·s [*Strehlau and Meissner*, 1987]. We will assume an average value of 10^{21} Pa·s. Other thermally activated power-laws are possible but will not be considered here [*Chopra and Paterson*, 1984].

3.4. Erosional and Depositional Processes

As mentioned in section 2, erosion and sedimentation rates in the Ventura basin were extremely high during the Pleistocene and therefore cannot be neglected. In our models we reproduce the behavior of the crust undergoing shortening of almost 10%. This amount of shortening is enough to produce significant displacements on the faults which, if erosion was not present, would lead to clearly unrealistic topography. Besides, the influence of mass transport on tectonic activity should not be neglected. We use an erosion-sedimentation model whose main parameters are pluviosity, intensity of river flow, and slope (details in Appendix B). We assume that mass is constant, despite the fact that sediment transport usually occurs in a direction perpendicular to the basin axis; thus the parameters that we used are not easily related to their natural counterparts. However, the implementation of this process enables the modeling of basin fill and provides a way of following the formation of the stratigraphic sequence, the latter being one of the main controls on the model's output. Two types of erosion will be used in the model. "Weak" erosion is our reference process, which takes into account river flow, pluviosity, and slope control. "Strong" erosion multiplies mass transport by 10, providing a more efficient basin fill and migration of the watershed.

3.5. Geometrical and Rheological Setup of the Model

As stated in the introduction, we discuss separately the formation of the San Cayetano fault and the process of subsidence of the Ventura basin. In the former case, two different aspects are considered: (1) the effect of erosion, rheology, and preexisting structures on the development of a strain localization zone, which mimics the San Cayetano fault and (2) the effect of sediment rheology on the geometry and the kinematics of the basin structure and the shear zones created. In the latter case the emphasis is on the relative strengths of the Oak Ridge and San Cayetano faults, when considered as fully developed frictional structures.

3.5.1. Formation of the San Cayetano fault. By modeling the compression of the Oak Ridge fault in a context of an asymmetrically thinned crust (Figure 3), we try to find a mechanical argument to explain the geometry of the San Cayetano fault at depth. All blocks presented in Figure 3 are initially intact, the only preexisting weaknesses (inherited from the initial extensional phase) being geometrical i.e. the presence of the Oak Ridge fault and a thin crust to the north. There is friction on the surfaces in contact along the Oak Ridge fault, with a friction coefficient $\mu \leq 0.35$. For boundary conditions we impose shortening at both sides of the model at a constant rate of 1 cm/yr, while the model lies in equilibrium over a dense viscous fluid (hydrostatic conditions at the base of the model). The initial width of the model is 120 km, and we model deformation to a depth of 35 km. The overall shortening of the model is 10 km (8.33%).

One of the key assumptions for this model is the south dipping geometry of the Oak Ridge fault. As this fault initiated

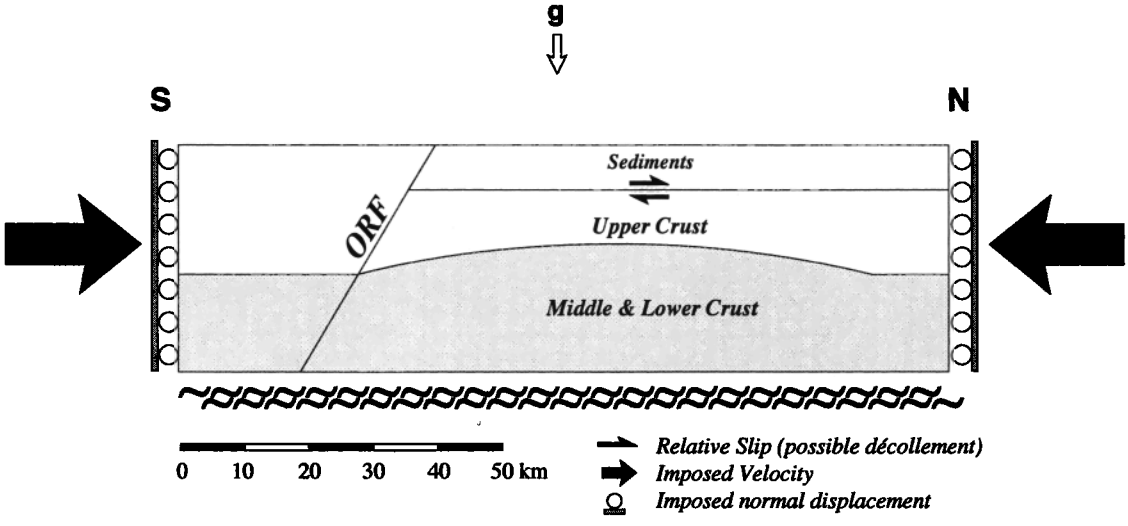

Figure 3. Mechanical model used to study the origin of the San Cayetano fault. The base of the model experiences hydrostatic pressure (represented by the "approximate" symbols). The relative slip marks the possible décollement surface used in some examples. When this décollement is not present, the interface acts as a deformation marker. In our numerical experiments the upper crust will always be elastoplastic and the sediments will be either elastoplastic with a low (φ=21°) or a normal (φ=30°) friction angle, or linear viscous. Friction along the Oak Ridge fault obeys Coulomb's friction law.

as a normal fault, it could possibly dip to the north. However, we believe that because of the major crustal rotations in the zone (of ~90°) [*Luyendyk*, 1991], it is possible that this fault completely changed its dip to become a south dipping fault 4 million years ago. Other interpretations [*Namson and Davis*, 1988] consider the possibility of a variable dip Oak Ridge fault: to a depth of 5-7 km the Oak Ridge fault is definitely south dipping (as confirmed by control wells), but at greater depths they believe this fault is still north dipping (a hypothetical south dipping blind thrust is also proposed to explain the observed topography). To explore the consequences of *Namson and Davis*'s [1988] hypothesis, we made a simulation to check if it was mechanically possible to find a south dipping Oak Ridge fault that changes dip at depth. We found that the problem with such a configuration is that under compression a pop-up block is created south of the Oak Ridge fault, as a prolongation of the deep branch of this section (see Figure 4). Such a feature would be clearly visible in the field and is not observed. Another interpretation is that the Oak Ridge fault separates into two branches at depth, the Oak Ridge fault and the Oak Ridge normal fault [*Huftile and Yeats*, 1995]; however, under compression the south dipping branch will always play the dominant role. Furthermore, the analysis of geodetic data [*Donnellan et al.*, 1993] provides a better fit when slip on faults of constant dip (as proposed in our mechanical model) are considered. These arguments provide a good degree of plausibility for our geometrical setup. Nevertheless, a complete treatment of this problem falls beyond the scope of this study and would certainly require the analysis of the three-dimensional behavior of the fault during the crustal rotations of southern California.

Assuming the geometrical setup shown in Figure 3, we have undertaken a parametrical study of the position and geometry of the generated strain localization zone that we associate with the San Cayetano fault. The parameters we have considered are both the position and width of the crust thinning as well as the strength (the friction coefficient) of the Oak Ridge fault. On the basis of observations, our main constraint is that only one strain localization zone (the San Cayetano fault) should be generated (instead of a pair of antithetic faults), with a northward dip and whose surface trace is at a distance of ~10 km to that of the Oak Ridge fault [*Huftile and Yeats*, 1996]. The optimal width of the thinned crust was found to be 80 km (as is shown in Figure 3), with its minimum thickness being 15 km, as constrained by seismic activity (although deep earthquakes of depth ~25 km have been documented in the zone [*Bryant and Jones*, 1992], this is not in contradiction with the results obtained, see section 4.4). The only effect of varying width is to displace the position of the strain localization zone to one side or another; strain localization almost always occurred with the expected dip direction (except in the extreme cases of a very wide or narrow anomaly where two antithetic bands appeared simultaneously).

3.5.2. Basin subsidence. If we accept that the San Cayetano fault has the subsurface geometry described by *Huftile and Yeats* [1996], we can use their retrodeformed cross section (simplified in Figure 2) as the starting point for the modeling of the behavior of the basin during the last million years, assuming that the zone of high strain localization that we associate with the San Cayetano fault becomes a fault zone (see section 3.5.1). In this case, we are interested in analyzing the competing effects of fault slip on the Oak Ridge and San Cayetano faults for filling the basin and generating the observed topography, after the San Cayetano fault has been created (from 1 m.y. to present time, steps

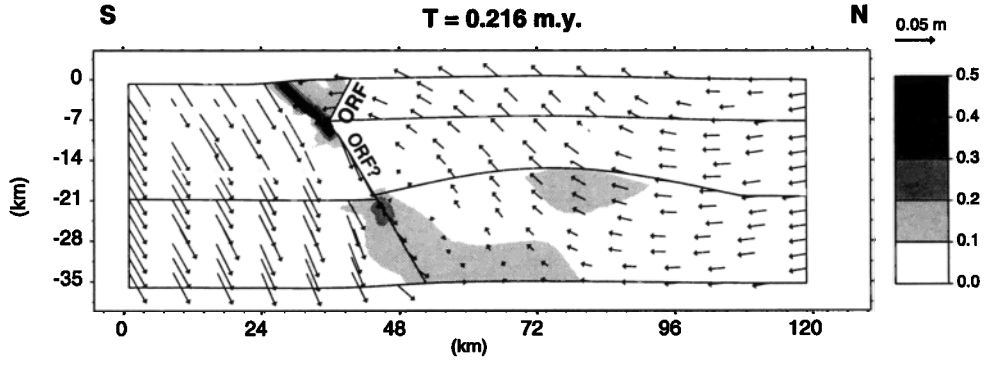

Figure 4. Results of the mechanical model used to study the effect of a variable dip Oak Ridge fault. Well data constrain this fault to be south dipping at the surface; however, its geometry at depth is discussed, as this was originally a normal fault and is expected to be north dipping. The mechanical setup is exactly the same as that of Figure 3, except that below a depth of 7 km the fault changes from southern to a 60° north dip. The starting point of the modeling is -4 m.y.; after only 0.216 m.y., a strain localization zone is developed, indicating that a fault is formed along the prolongation of the hypothetically north dipping Oak Ridge fault. We plot with a gray scale the intensity of deformation (second invariant of the deviatoric strain tensor) while the arrows indicate the displacement field. Such a geometrical setup subject to compression creates a pop-up structure that is not observed on the field, providing an argument against a north dipping Oak Ridge fault at depth.

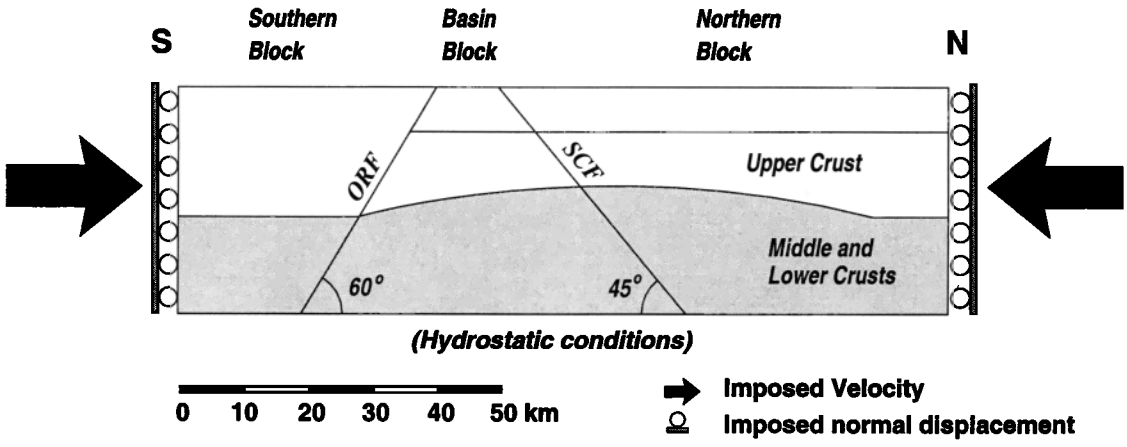

Figure 5. Mechanical model used to study the subsidence of the Ventura basin. The configuration is very similar to that of Figure 3. We suppose here that 1 m.y. ago the Oak Ridge and San Cayetano faults were fully developed and can be considered as frictional surfaces obeying Coulomb's friction law. We study the influence of the relative strengths of these faults on the shape of the generated basin and the way the basin subsides.

$c \Rightarrow a$ in Figure 2). As described in section 3.1, this analysis is done by treating the faults as purely frictional surfaces obeying Coulomb's friction law, where deformation is absorbed both by slip on the faults and by strain in the surrounding medium. The mechanical model used is shown in Figure 5. We impose a shortening rate of 1 cm/yr, the duration of the experiment being 1 m.y. We study the variation of strength (friction coefficient) of the San Cayetano fault while leaving that of the Oak Ridge fault fixed to the value that gives the "best fit" for the formation of the San Cayetano fault.

4. Results

We will obviously not present the results of all our experiments but rather concentrate on the most significant ones. For the study of the formation of the San Cayetano fault by strain localization, we present the results of the variations of three basic parameters: the friction coefficient μ on the Oak Ridge fault, the rate of erosion (weak or strong) and the presence or absence of a décollement in the northern block (under the Modelo formation, at a depth of 7 km). Since we seek to maximize the effects of the décollement surface for making them clearly visible, we have chosen to impose on it a very weak friction coefficient of $\mu = 0.05$. The other mechanical parameters are given in Table 1. The results of our numerical experiments are presented in Figures 6-9, where we show the intensity of the deviatoric strain tensor (which directly shows the amount of deformation or strain localization), the generated topography, the topography that would be present if no erosion or sedimentation were present, and the amount of fault slip on the Oak Ridge fault. The case where a décollement was present between the deep upper crust and the layer of sediments is also considered. Total slip along this décollement surface is shown under each décollement model. Our reference case is deformation with weak erosion and no décollement surface (a minimum of erosion is needed to ensure the continuity of topographical slopes and allow basin fill). In figures 6-9, even if no décollement is present, the 7 km interface between sediments and the rest of the upper crust is maintained as a passive marker of deformation. Even though we have studied many other cases ($\mu = 0.15$, 0.20, 0.25, 0.30, and 0.35), we will present only those where qualitative differences can be seen.

For the analysis of subsidence there is no need to show the evolution of the geometry of faults at depth, as it is imposed. In this case, the relevant parameter is the relative strength of the San Cayetano and Oak Ridge faults. We present both the topographic-basin profiles (Figure 10) and the slip on both faults (Figure 11) for the six cases analyzed.

4.1. Development of Strain Localization Zones: Erosion, Friction and Décollement Effects

4.1.1. Cases 1-3: $\mu = 0.15$ (Figure 6). In case 1 the experiment with weak erosion, we can clearly see that the Oak

Table 1. Parameters of the Numerical Experiments

Case	μ_{ORF}	Erosion	Décollement	Figure
1	0.15	Weak	Absent	6
2	0.15	Strong	Absent	6
3	0.15	Strong	Present	6
4	0.25	Weak	Absent	7
5	0.25	Strong	Absent	7
6	0.25	Strong	Present	7
7	0.35	Weak	Absent	8
8	0.35	Strong	Absent	8
9	0.35	Strong	Present	8

All sediments are elastoplastic with $\varphi = 30°$.

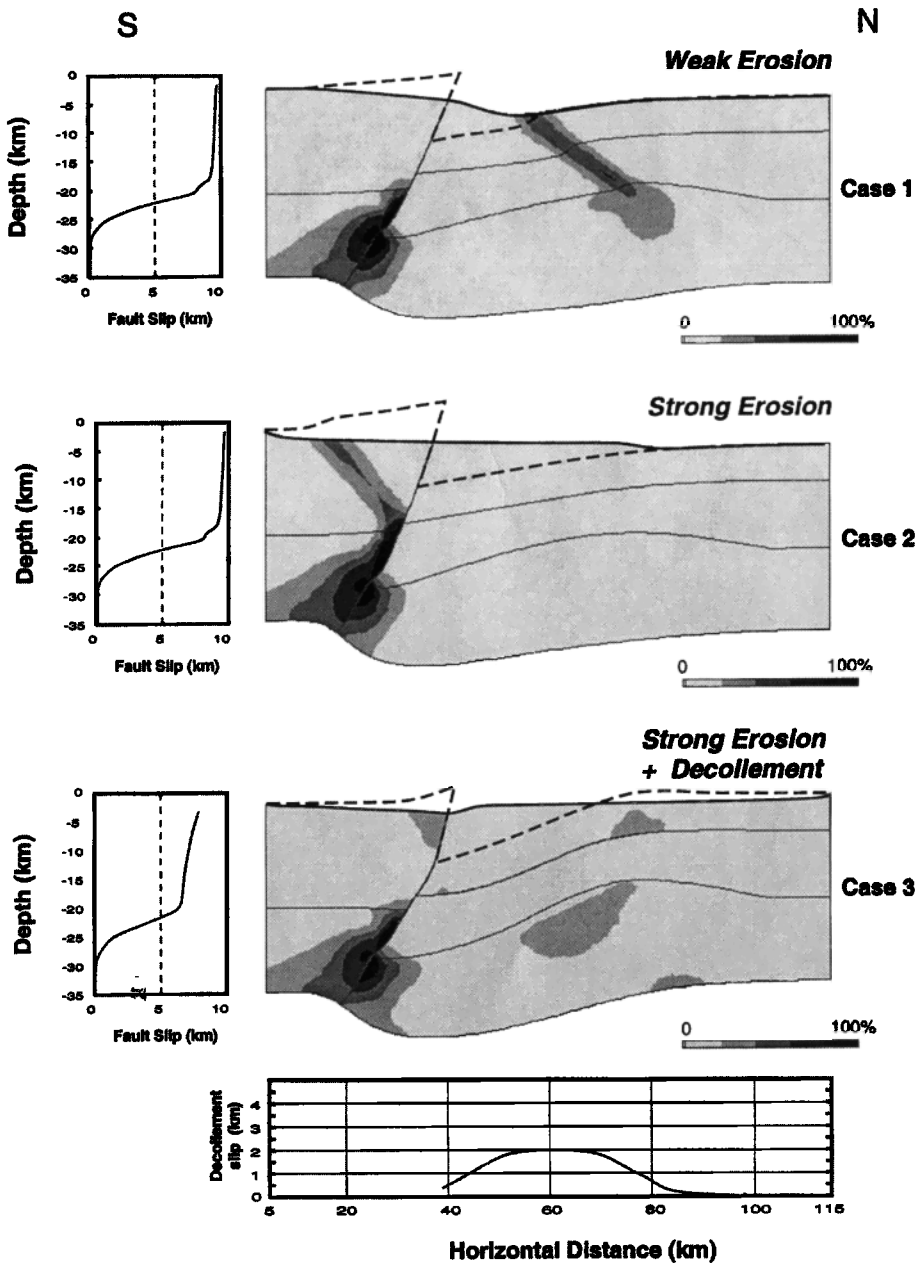

Figure 6. Total strain in the Ventura basin for an Oak Ridge fault (ORF, south dipping of strength μ_{ORF} = 0.15) in a roughly S-N cross section. The gray scale shows the intensity of deformation (second invariant of the strain tensor); thus black zones correspond to strain localization regions (i.e. shear bands/faults). Fault slip on the Oak Ridge fault is shown at the left of each case. Décollement slip (at the 7 km depth interface of case 3) is shown in the lower plot. Superposed on the cross section, the dashed line shows the topography that would exist if no erosion or sedimentation were present (see Table 1 for parameters used).

Ridge fault is so weak that most of the shortening is absorbed by displacement on this fault. The 10 km shortening creates an almost 10 km slip on the Oak Ridge fault. The activation of a strong erosional process (case 2) does not change the slip rate of the Oak Ridge fault; however, it does significantly modify the shape of the basin, and strain localization takes place in the southern block instead of in the northern one. In case 3, where a décollement is present, a total of nearly 8 km slip is observed on the Oak Ridge fault, with a 2 km slip on the décollement surface. Deformation imposed by shortening is absorbed mainly by slip on these two surfaces, creating a rather homogeneous overall deformation.

4.1.2. Cases 4-6: μ = 0.25 (Figure 7). Increasing the strength of the Oak Ridge fault has the obvious effect of diminishing slip along it. In all three cases the strain localization zone formed occurs roughly at the same place, at

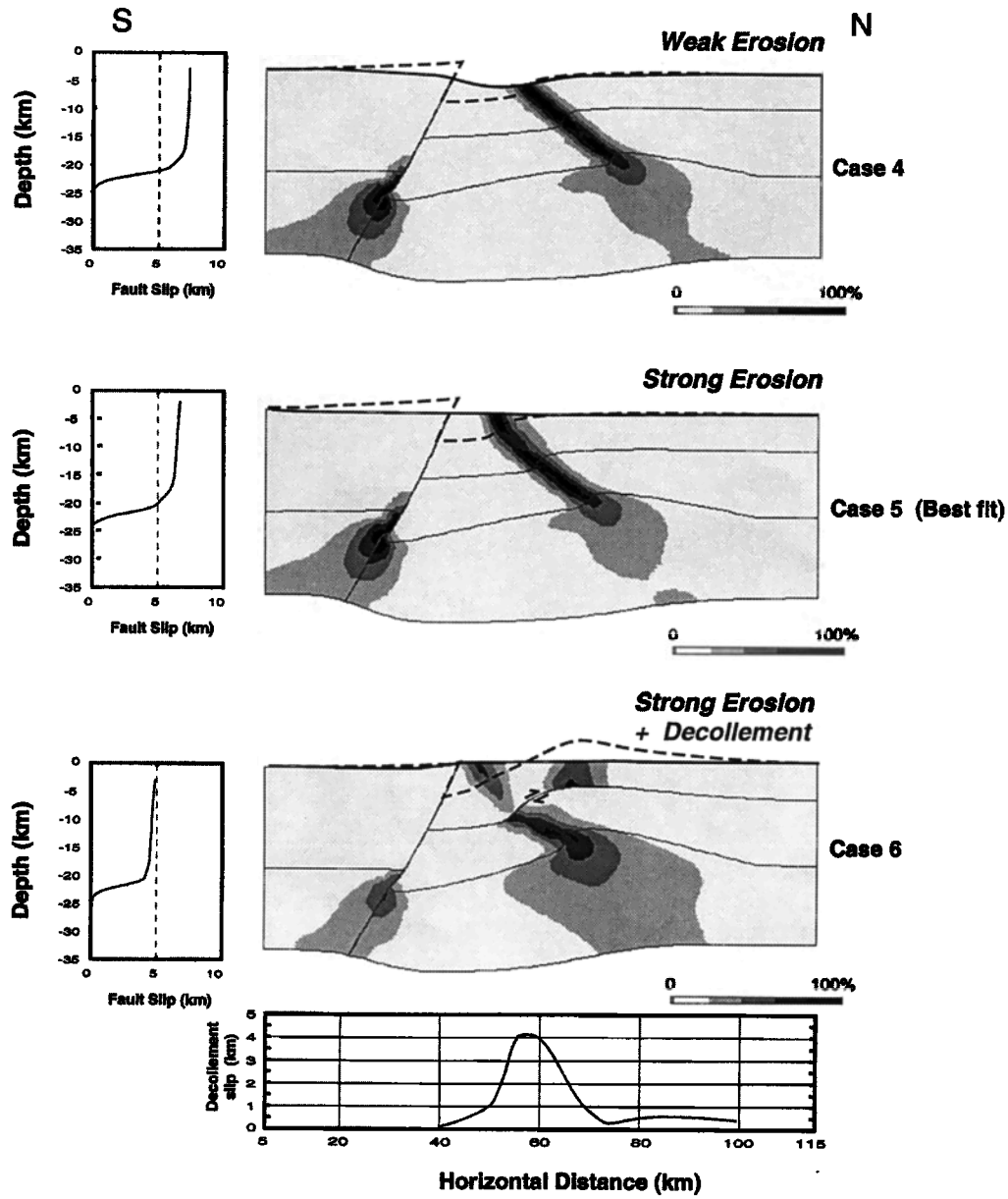

Figure 7. Same as Figure 6, but for $\mu_{ORF} = 0.25$.

~10 km north of the Oak Ridge fault (at the surface), its dip being between 45° and 50°. The main difference between cases 4 and 5 is the shape of the basin; in the former the basin has a width of 20 km, while case 5 creates a deeper and narrower basin. For the décollement model (case 6), deformation is more easily absorbed by the décollement surface, which slips twice as much as when $\mu = 0.15$ (case 3). We observe the formation of a low-angle fault beneath the décollement, which steepens after passing the décollement interface and a second zone of localization, ~15 km north of the basin.

4.1.3. Cases 7-9: $\mu = 0.35$ (Figure 8). A further increase in the friction coefficient locks the Oak Ridge fault. Slip along this fault is virtually zero, except for case 7 (weak erosion), where the thickening of the crust is accompanied by a (relatively) small slip along the Oak Ridge fault. A negligible amount of deformation is absorbed by slip on the Oak Ridge fault, so bulk deformation is much more intense than in the other cases the result being that sediments overflow the basin (no attempt to modify the "standard" parameters of erosion was made). In cases 7 and 8, a pair of antithetic shear zones is formed, though the northward dipping one (San Cayetano) predominates. In case 9, deformation is more easily absorbed by slip on the décollement surface; relative slip attains the value of 11 km (the greatest slip observed in cases 1-9).

4.1.4. Discussion of cases 1-9. The San Cayetano fault is modeled as a strain localization zone; we are more con-

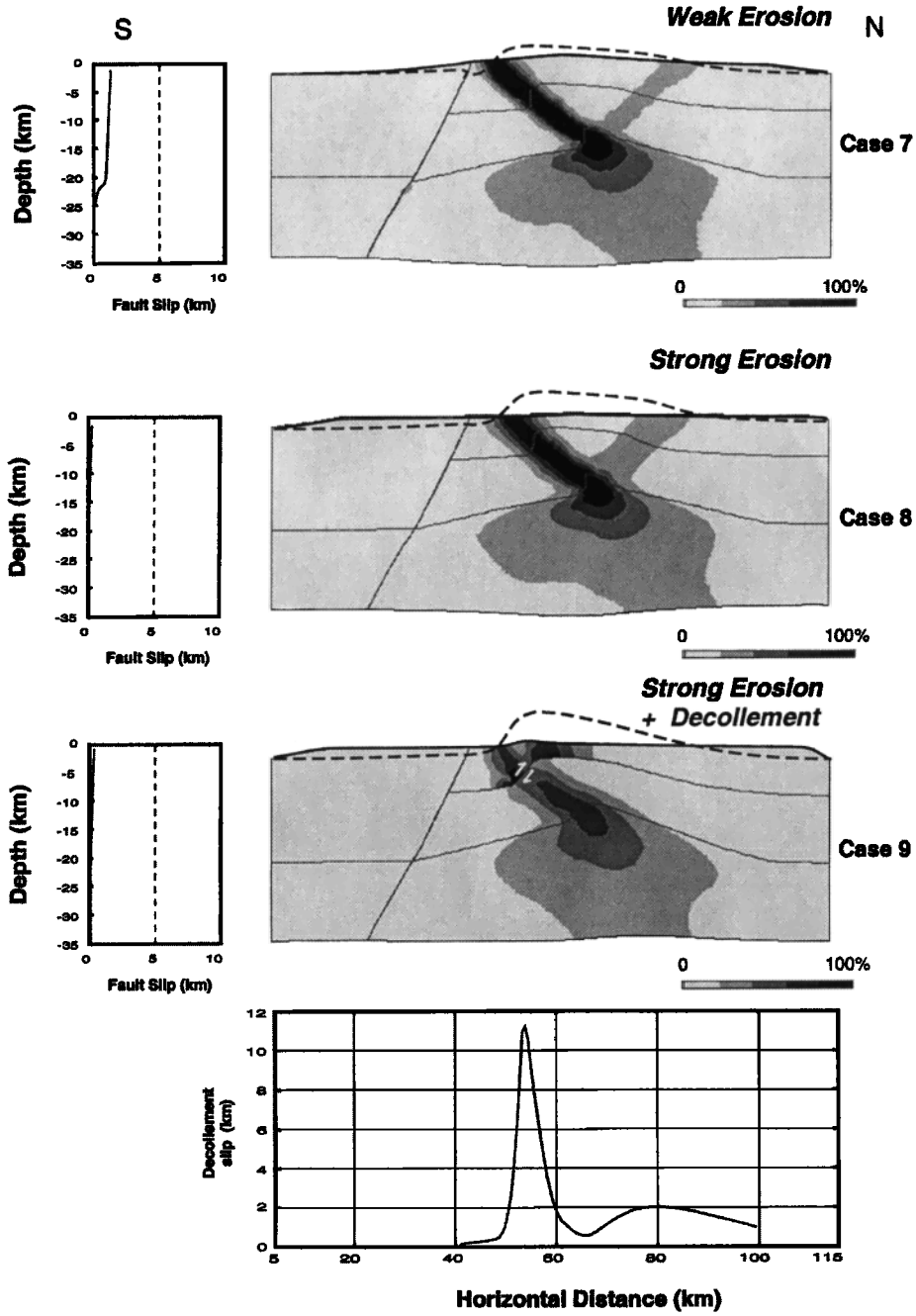

Figure 8. Same as Figure 6, but for $\mu_{ORF} = 0.35$.

cerned with obtaining information on what conditions its position and geometry (the compressional event between 3-4 and 1 m.y., Figures 2d and 2c) than its tectonic activity. Nevertheless, we can evaluate the results of our models by comparing the overall shape of the generated basins and topography with the information we have from actual geological and geophysical surveys (Figures 1b and 1c). Of these criteria, basin shape is the most significant, since topographical elevation strongly depends on the initial configuration of the system, which we have assumed to be flat. However, a very marked general trend in topography can still be meaningful. The general behavior of the watershed is also worth noting. It is clear that cases 1-3 ($\mu = 0.15$) and 4 ($\mu = 0.25$) create a basin that is far too wide, compared to reality (Figure 1b). Cases 5 and 6 ($\mu = 0.25$) give a more plausible picture of the basin. Case 5, $\mu = 0.25$ and strong erosion, provides the best fit with basin shape, width, and position of the San Cayetano fault. In this case, however, topography is not correct. Contrary to observations, in this simulation the southern shoulder of the basin predominates over the north-

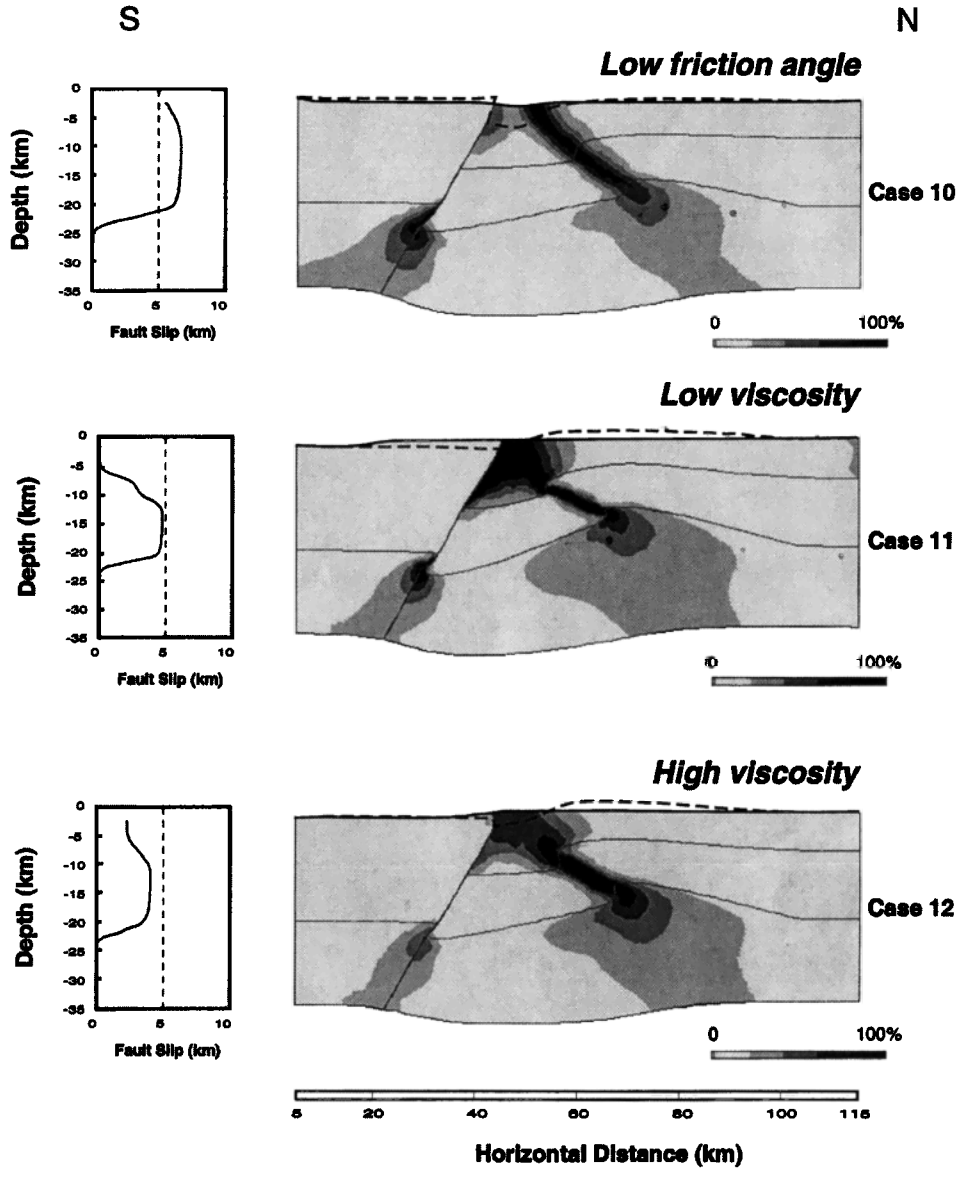

Figure 9. Same as Figure 6, but for $\mu_{ORF} = 0.25$ and a weak sediment layer. In case 10 the sediments are elastoplastic with a low internal friction angle. In cases 11 and 12, sediments are linear viscous (see Table 2 for parameters used).

ern one. Case 6 (décollement with $\mu = 0.25$) creates a basin whose base is very asymmetrical in shape and with opposite slope to that observed. However, it is interesting to note the striking resemblance of this case with cross section BB' (Figure 1c). In this parametrical study the best fit is case 5, and it will be the starting point for a refinement of our model, where different rheologies for sediments will be used.

4.2. Geometry of the Basin: Sediment Rheology Effect

Using the results of the best case of section 4.1 ($\mu = 0.25$ with strong erosion), we study the effect of using a different rheology for the layer of sediments on the northern block. As discussed before (section 3.3), two approaches are possible: either an elastoplastic rheology with a low friction angle or a viscous rheology. Both possibilities are studied using the three cases described in Table 2.

4.2.1. Case 10: $\mu = 0.25$, sediments with low friction angle (Figure 9). As the sediments overlying the Modelo formation (7 km thickness) have been identified as an alternating sequence of shales and sandstones, we can model their behavior by using the Drucker-Prager elastic-plastic rheology with a smaller friction angle than the standard value of 30°. The experimental data of a variety of shales and sandstones *Handin and Hager* [1957, 1958] can be reproduced numerically by using friction angles between $\varphi =$ 17° (Green River shale) and $\varphi = 27°$ (Barnes sandstone). We shall assume an intermediate value of $\varphi = 21°$ for the

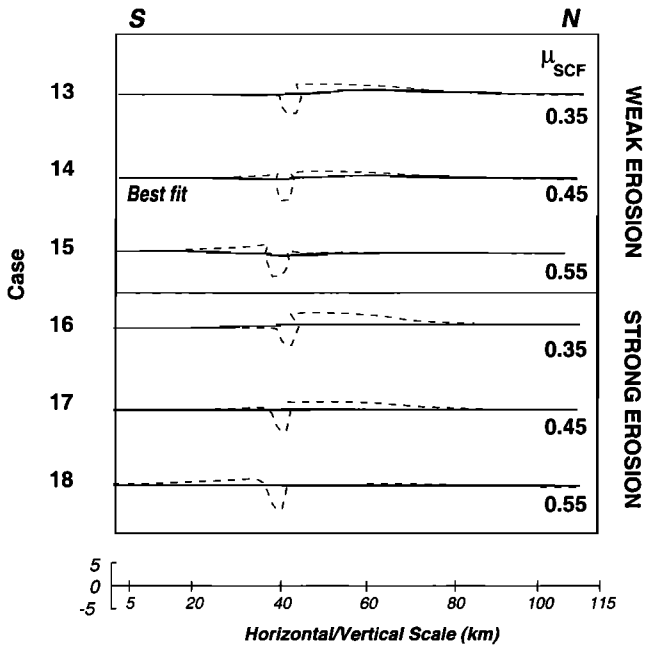

Figure 10. Profiles of the basins created in cases 13-18, for the modeling of subsidence on the Ventura basin. See text for discussion and Table 3 for parameters used.

sediment layer of case 10. The model shows a slight fault slip damping near the surface, as well as a moderate strain localization within the basin.

4.2.2. Cases 11-12: μ = 0.25, viscous sediments (Figure 9). We have no a priori information of the value of viscosity that we should use to model the sediment layer, but it seems plausible that it should be no greater than 10^{21} Pa·s, the value used to model the middle and lower crust. We use two values of viscosity that produce qualitatively different results; as in cases 7-9, there is sediment overflow. In case 11, a low-viscosity layer of sediments ($\eta = 10^{20}$Pa·s) is used. The qualitative result is completely different from both case 10 and the reference case. The north dipping strain localization zone that is formed at depth is flat and is connected to a relatively shallow basin that suffers intense deformation and thickening, with virtually no topography. Slip on the Oak Ridge fault is completely attenuated at the surface (above 4 km depth). In case 12, with a higher viscosity ($\eta = 10^{21}$Pa·s), the qualitative result is relatively similar to case 11, but there is much less damping of fault slip at the surface. The San Cayetano fault at depth shows approximately the same dip. The basin is deeper than that in case 11, but again erosion has completely erased the topographic profile of the basin.

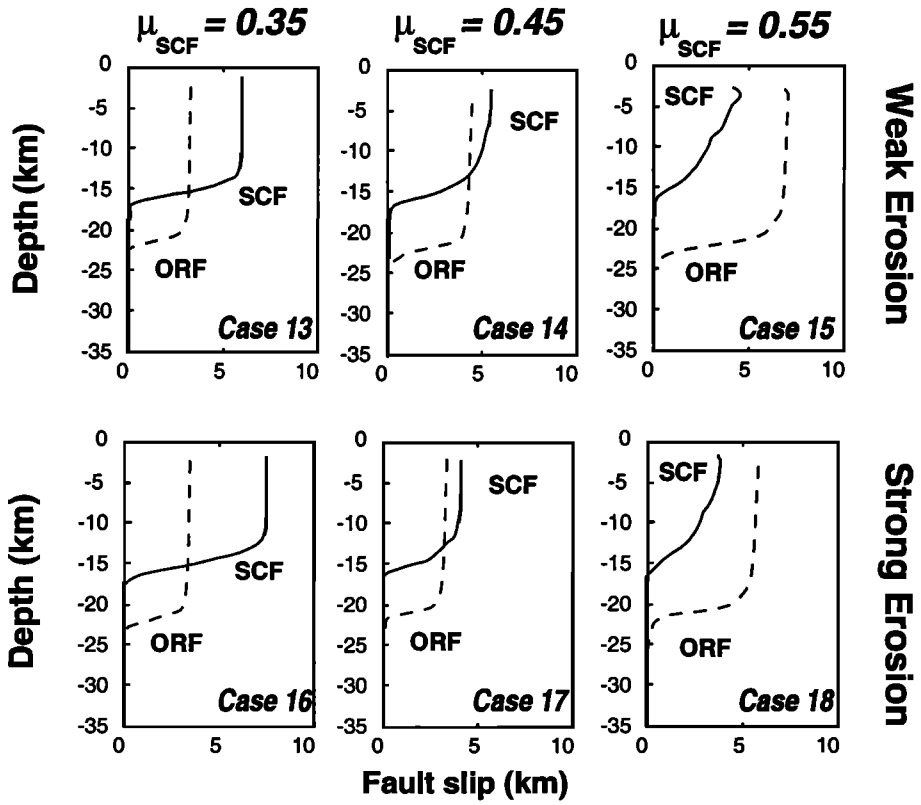

Figure 11. Slip versus depth in cases 13-18, while both the coefficient of friction along the San Cayetano fault (the Oak Ridge fault is assumed to have a constant friction coefficient of 0.25) and the rate of erosion in the basin are varied. On the basis of basin shape and topography height, the best fit is found to be case 14. See text for discussion and Table 3 for parameters used.

Table 2. Numerical Parameters for the Weak Sediments Experiments

Case	μ_{ORF}	Erosion	Décollement	Sediments	Figure
10	0.25	Strong	Absent	$\varphi = 21°$	9
11	0.25	Strong	Absent	$\eta = 10^{20}$*	9
12	0.25	Strong	Absent	$\eta = 10^{21}$*	9

*Units are pascals·seconds.

4.3. Basin Subsidence: Effect of the Relative Strength of the Oak Ridge and San Cayetano Faults

We consider the effect of varying the strength of the San Cayetano fault, once it is a fully developed frictional surface (the last 1 m.y.). The value of friction on the Oak Ridge fault is that of the best fit of section 4.1, i.e., $\mu_{ORF} = 0.25$. The parameters used are shown in Table 3; the effects of erosion are also taken into account. The main criterion for establishing a "goodness of fit" in these models is the overall shape of the basin and the position of the watershed.

4.3.1. Cases 13-15: Weak erosion (Figures 10 and 11). In case 13, the strength of the San Cayetano fault is too low to avoid dominant slip on its surface, almost twice as much as the slip on the Oak Ridge fault. Case 14, with $\mu_{SCF} = 0.45$, is almost an equilibrium situation, slip on the Oak Ridge and San Cayetano faults being comparable. Increasing the San Cayetano fault's strength diminishes slip on it significantly, while slip mainly takes place on the Oak Ridge fault. The depth of the basin in all three cases is approximately the same, ranging from 4000 to 4500 m. The main difference between these 3 cases is mostly seen in the topography. As shown in Figure 10, the low-strength San Cayetano fault of case 13 creates high relief to the north, almost flat to the south. With $\mu_{SCF} = 0.55$, fault slip on the Oak Ridge fault creates a dominant topography to the south, the inverse of what is seen in the field. Intermediate case 14 can be shown to be the best case, topographical relief being comparable to that shown on Figure 1b.

4.3.2. Cases 16-18: Strong erosion (Figures 10 and 11). As in cases 13-15, increasing strength on the San Cayetano fault diminishes fault slip on this structure, while increasing slip on the Oak Ridge fault. Qualitative results are the same as in cases 13-15. The generated topography is in fact very different to the case of weak erosion, concerning absolute altitudes. However, the main fact is that the dominant character of the southern or northern topography is the same in both models and, hence, does not depend greatly on the details of the erosion-sedimentation algorithm.

An example of how the subsidence takes place through time is shown in Figure 12, showing three snapshots of the deviatoric stress and the displacement vectors after 0.25, 0.5, and 1 m.y. of simulation (i.e., from -0.75 m.y. to present time). Note that there is a small discontinuity in displacement between the southern block and the basin, while there is a big difference in the relative displacements of the basin and the northern blocks.

4.4. Discussion

The results of our modeling seem to indicate that the presence of weak sediments in the northern block of the Ventura basin system does influence the shape of the basin. Of the values tested, the most "realistic" results were obtained with elastoplastic sediments having a low friction angle. In this experiment (case 10), the observed width of the basin is roughly 10 km, the value calculated for -1 m.y. [*Huftile and Yeats*, 1996]. In our model, low-viscosity sedimentary layers create a basin that absorbs slip on the Oak Ridge fault, while extending deformation to the base of the brittle-ductile transition. The same is also true for high-viscosity sediments, except in this case, slip on the Oak Ridge fault does reach the surface.

Most north dipping strain localization zones created in our models dip between 40° and 50°. One remarkable exception is the décollement model of case 6 (and to a lesser extent, that of case 9). Its presence creates an important flexure at the base of the décollement surface, which seems to be responsible for an abrupt change in dip of the shear zone, increasing above the décollement level and decreasing under it. The resulting fault geometry closely resembles cross section BB' of Figure 1c. Close to this profile an abnormally thick sequence and the dipmeter readings of the Taylor 653 well (passing beneath the Ventura Avenue Anticline) indicate the possible presence of a décollement under this anticline [*Yeats*, 1983]. The present result of these models is another argument for considering the existence of a décollement under the east central Ventura basin. If this is so, one possible important effect is the presence of a low-angle fault at depth, which steepens near the surface.

Sediment viscosity seems to play a very important role in fault slip. We have observed in our models that the presence of low-viscosity sediments can completely damp fault slip so as to make it zero at the surface, even when fault slip continues at depth. There is a qualitative difference in behavior for viscosities between 10^{20} and 10^{21} Pa·s, the former stopping fault slip on the Oak Ridge fault and the latter propagating it. However, even if this qualitative jump exists in nature, the actual values of viscosity are expected to be different from those presented because of all the simplifications that we have assumed when establishing our models.

Table 3. Parameters of the Experiments of the Frictional Approach

Case	μ_{ORF}	μ_{SCF}	Erosion	Figure
13	0.25	0.35	Weak	10 and 11
14	0.25	0.45	Weak	10 and 11
15	0.25	0.55	Weak	10 and 11
16	0.25	0.35	Strong	10 and 11
17	0.25	0.45	Strong	10 and 11
18	0.25	0.55	Strong	10 and 11

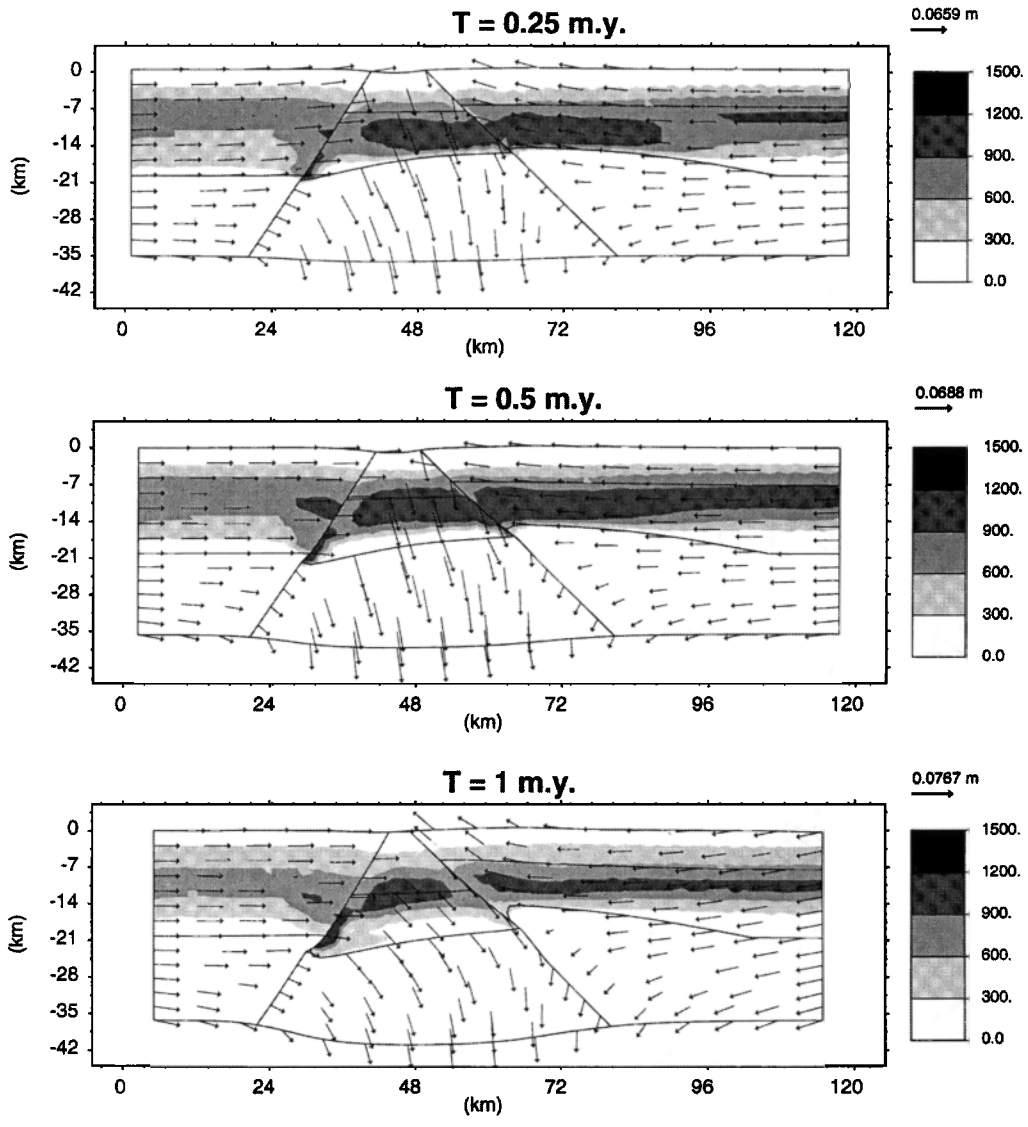

Figure 12. Images of three stages of subsidence for the best fit of cases 13-18. Note the discontinuity in displacement vectors on both sides of the San Cayetano fault. Unlike Figure 4, we show on a gray scale the intensity of the deviatoric stress (second invariant of the deviatoric stress tensor), its magnitude being shown in megapascals on the scale at right. The arrows indicate the displacement field.

As stated in the discussion of the geometrical setup (section 3.5), deep earthquakes have been recorded in the Ventura basin [*Bryant and Jones*, 1992]. It is easy to see by looking at Figures 6-9 that after deformation the base of the basin is found at depths ~25 km and our models are hence compatible with these observations.

The relative strengths of the Oak Ridge fault (ORF) and San Cayetano fault (SCF), control the activity of these faults and the related uplift. Using our fault geometry, the effective friction coefficient of the San Cayetano fault should be much higher than that of the Oak Ridge fault. For a fixed value of strength of the Oak Ridge fault ($\mu_{ORF} = 0.25$, the best fit of the strain localization analysis), the most realistic generated topography is obtained for $\mu_{SCF} = 0.45$ and weak erosion. The Oak Ridge fault therefore appears to be more lubricated than the San Cayetano fault, as is expected for an older fault. Sediment thickness and basin subsidence are very similar for all cases, all being compatible with observations.

Intuitively, the San Cayetano fault must be much stronger than the Oak Ridge fault; if this were not the case, because of its shallower dip, most deformation would be absorbed by slip on this fault thus generating a very steep topography on the northern side (Topatopa mountains). Our modeling shows that this is indeed the case, the qualitative change in behavior occurring for $\mu_{SCF} \approx 0.45$. However, we must bear in mind that this is true under the major assumption that the strength of the Oak Ridge fault is $\mu_{ORF} = 0.25$. It is almost certain that the resulting topographic configuration depends more on the ratio of these strengths than on their absolute value. However, this strength ratio is also a function of the

dip ratio of the faults. If the dip of the San Cayetano fault is lower than the one we took, the SCF/ORF strength ratio must be even higher. However, values for μ cannot be arbitrary, an upper limit being given by the tangent of the angle of internal friction and the value of μ_{ORF} having been constrained in the continuum approach modeling of the Ventura basin.

Again, these values are only average values used in our models; the actual values of the friction coefficient in nature can be different and even depth dependent. In the field the maximum altitudes in the area spanned by our model are of ~1000 m to the north and 400 m to the south; case 14 can be selected on those grounds as providing the best fit (sediment thickness being comparable for cases 13-18). Furthermore, one can say that being an older fault, the Oak Ridge fault should be better lubricated than the younger San Cayetano fault and thus should have a lower strength than the San Cayetano fault, an argument that agrees with our results.

5. Conclusion

We have presented a model of the behavior of the east central Ventura basin, which allows us to study the simultaneous effects of the response of a faulted crust to compression, erosion and sedimentation, and fault activity. We use a continuum approach with an embedded frictional fault (the Oak Ridge fault) to study the conditions under which strain localization could have occurred in the crust to create the San Cayetano fault; this may model the beginning of the shortening process (steps $d \Rightarrow c$ in Figure 2), from -4 to -1 m.y. As in all types of modeling, the conclusions obtained are valid only within the framework of the model. The major assumption that we have made, other than the average rheological behavior described in section 3.3, is the assumption that the evolution of the geological system can be modeled in quasi-static conditions. Furthermore, we assume that the Oak Ridge fault is a preexisting fault of constant southern dip, that the geometry of the brittle-ductile transition under the northern block we have supposed is correct, and that initial topography on the zone was negligible. With these limitations in mind, several conclusions can nevertheless be drawn from our models:

1. The mechanical models constructed using a south dipping Oak Ridge fault at depth provide results which are consistent with available data. The activity of a deep north dipping Oak Ridge fault has been shown to be mechanically inconsistent with structural observations (although its presence has not been ruled out).

2. Compression of a system consisting of a preexisting fault (Oak Ridge fault) and a crustal thinning (north of the Oak Ridge fault) are sufficient conditions for the creation of an antithetic thrust fault (San Cayetano fault), which allows a large basin subsidence. In our model a crustal thinning 40 km north of the Oak Ridge fault creates a strain localization band at the place where the San Cayetano fault is found.

3. The parametrical study that has been carried out constrains the effective friction of the Oak Ridge fault to be between 0.15 and 0.35 in order to get a basin shape and topography consistent with current observations.

4. There is a need to involve relatively major erosion (2-3 km) and sedimentation (5 km) to reduce topographic amplitude toward realistic values, fill the basin and obtain a good fit on basin shape.

5. The presence of a décollement level (under the Modelo formation, at a depth of 7 km) can induce the formation of a fault having a low-angle dip below the décollement and a high-angle dip above it (case 6). This angular offset is accommodated by the décollement, itself acting as a backthrust.

6. When weak sediments are included in our modeling, the main result is that a low internal friction angle gives a better fit on basin geometry and that viscous sediments can be the cause of a flat and buried fault (no slip at the surface, despite fault activity at depth). For a critical viscosity between 10^{20} and 10^{21} Pa·s, a qualitative change in behavior has been observed. The topographic response of the model precludes the use of effective viscosities lower than 10^{21} for the sediments, since they lead to basin thickening and therefore inhibit subsidence.

7. In our second model a frictional discontinuous approach to the interaction of the Oak Ridge and San Cayetano faults permits us to quantify the relative strengths of these faults and model the main phase of shortening (steps $c \Rightarrow b \Rightarrow a$ in Figure 2), from -1 m.y. to the present. On the basis of the qualitative shape of the basin and the position of the watershed, we found that the best fit was that of case 14, with weak erosion and relative fault strengths of $\mu_{ORF}/\mu_{SCF} = 0.25/0.45$. We also observed that in an initial phase the southern block and the basin subside at the same rate (while the fault is still locked), while later both the southern and northern blocks move upward relative to the basin block.

8. The results presented in this study appear to be compatible with all available data and thus provide another argument in favor of a south dipping Oak Ridge fault at depth (although the existence of an inactive north dipping branch and a slightly variable dip have not been ruled out).

Appendix A: Remeshing Criteria

The quadrilateral elements used in our finite element method analysis are composed of pairs of triangular elements. The accuracy and stability of numerical computations of strain localization, depend to a great extent on the good numerical behavior of the spatial discretization and in particular on how precisely the variations in the states of strain and stress can be described. This is directly related to the size and shape of each and every element. The relationship between element size and precision is obvious. The shape of the element is also important, as the calculations done at

the element nodes are interpolated throughout its volume via the shape functions which are optimal for a given geometry. Hence a "bad" geometry can lead to physically imprecise results.

The quality of such quadrilateral mesh is that of the poorest triangular element in it. The quality Q of an individual element is proportional to the ratio of the length $L_{\max}$ of the longest side of the triangle, and the radius R of the maximum inscribed circle, in such a way that a rectangular isosceles triangle has a quality factor Q of 1:

$$Q = \frac{\tan(\pi/8)}{\sqrt{2}} \frac{L_{\max}}{R} \qquad \text{(A1)}$$

Note that a bigger value of Q indicates an increasingly bad geometry. In the case of sedimentation and erosion, the shape of the elements is modified to account for increasing or decreasing volume. This change of shape modifies the quality factor and is also true for elements undergoing strain. By monitoring the evolution of the quality of the mesh, at the same time we control the accuracy of the solution. The remeshing process in these simulations was triggered either when this quality factor Q was greater than 2.8 or when the surface area of an element changed by more than half its initial value.

Appendix B: Erosion and Sedimentation Processes

Supposing that the mass is constant throughout the experience (although mass transport takes place essentially in a direction perpendicular to the basin axis), we calculate the eroded or sedimented mass as a function of slope and river flow, by solving the one-dimensional diffusion equation. To solve this equation, we need to define the topography (initially zero, then given by the geodynamical calculation) and a diffusion coefficient at each point i on the surface to be eroded. We calculate the diffusion coefficient at point i ,Q_i, as a function of the altitudes of its neighbors, times a transport coefficient C_T, which takes into account both pluviosity and river transport (equation B1). The total diffusion coefficient will then be modified to enhance the diffusion of high slopes (as compared to a critical slope, slope_c ; Q_o is a minimal slope diffusivity) but limiting its value by the exponential term that fixes a characteristic length of transport C_R (equation B2). This recursive equation is then solved at each time step by implicit integration, giving the new altitudes of the eroded surface:

$$Q_i = f\left(\text{altitude}_{i-1}, \text{altitude}_{i+1}\right) C_T \qquad \text{(B1)}$$

$$Q_i = Q_0 \left(1 + \frac{\text{slope}}{\text{slope}_c}\right)^2 + Q_i \left(1 - e^{-Q_i/(C_T C_R)}\right) \qquad \text{(B2)}$$

Erosion is modeled by diminishing the surface area of eroded elements, while sedimentation is simulated by increasing the surface area of elements where sediments are to be deposited. Therefore sedimented layers have the same rheology as that of the surface on which they are on. When the surface area of an element is less than half of its initial value, remeshing is undertaken to ensure the stability of the computation by avoiding poor-quality elements.

Acknowledgments. This is BRGM contribution 96047. This work was financially supported by a BRGM research grant (F.N.) and by the Southern California Earthquake Center (J.P.G.). We are grateful for the invaluable technical help from Riad Hassani. Michel Jean provided us his implementation of the contact-friction algorithm, and Francis Lucazeau provided us his erosion-sedimentation code. We are very grateful for the comments of S. Ellis and R. Yeats which helped to greatly improve this manuscript, and for the corrections of English style by K. Hardacre.

References

Ben-Menahem, A., and S. Singh, Multipolar elastic fields in a layered half space., *Bull. Seismo. Soc. Am., 58*, 1519–1572, 1968.

Bills, B., D. Currey, and G. Marshall, Viscosity estimates for the crust and upper mantle from patterns of lacustrine shoreline deformation in the eastern great basin, *J. Geophys. Res., 99*, 22,059–22,086, 1994.

Board, M., *FLAC (Fast Lagrangian Analysis of Continua) v2.20: Software Summary*, Itasca Consult, Group, Minn., 1989.

Brace, W., and D. Kohlstedt, Limits on lithospheric stress imposed by laboratory experiments, *J. Geophys. Res., 85*, 6248–6252, 1980.

Bryant, A., and L. Jones, Anomalously deep crustal earthquakes in the Ventura basin, southern California, *J. Geophys. Res., 97*, 437–447, 1992.

Butler, R., The influence of pre-existing basin structure on thrust system evolution in the western Alps, in *Inversion Tectonics*, edited by M. A. Cooper and G. D. Williams, vol. 54 of *Sp. Publ. Geol. Soc.*, pp. 105–122, Blackwell Sci., London, 1989.

Carter, N., and M. Tsenn, Flow properties of the continental lithosphere, *Tectonophysics, 136*, 27–63, 1987.

Chopra, W., and M. Paterson, The role of water in the deformation of dunite, *J. Geophys. Res., 89*, 4183–4224, 1984.

Crouch, J., and J. Suppe, Late cenozoic tectonic evolution of the Los Angeles basin and inner California borderland: A model for core complex crustal extension, *Geol. Soc. Am. Bull., 105*, 1415–1434, 1993.

Cundall, P., Numerical experiments on localization in frictional materials, *Ing. Arch., 58*, 148–159, 1989.

Davis, T., and J. Namson, A balanced cross-section of the 1994 Northridge earthquake, southern California, *Nature, 372*, 167–169, 1994.

Donnellan, A., B. Hager, and R. King, Discrepancy between geological and geodetic deformation rates in the Ventura basin, *Nature, 366*, 333–336, 1993.

Feigl, K., et al., Space geodetic measurement of crustal deformation in central and southern California, 1984-1992, *J. Geophys. Res., 98*, 21,677–21,712, 1993.

Gratier, J., Displacement field and geometric compatibility using computational restoration of folded and faulted strata: application to the last 3-4 ma in the Ventura and Los Angeles basin (abstract), *Eos, Trans. AGU, 76*, Fall Meeting Suppl.,143, 1995.

Gratier, J., and J. Gamond, Transition between seismic and aseismic deformation on the upper crust, in *Deformation Mechanism, Rheology and Tectonics*, edited by R. Knipe and

H. Rutter, vol. 54 of *Sp. Publ. Geol. Soc.*, pp. 461–474, Blackwell Sci., London, 1990.

Handin, J., and R. Hager, Experimental deformation of sedimentary rocks under confining pressure tests at room temperature on dry samples, *Am. Assoc. Petr. Geol. Bull.*, *41*, 1–50, 1957.

Handin, J., and R. Hager, Experimental deformation of sedimentary rocks under confining pressure: tests at high temperature, *Am. Assoc. Petr. Geol. Bull.*, *42*, 1958.

Hassani, R., Modélisation numérique de la déformation des systèmes géologiques, Ph.D. thesis, Univ. Montpellier II, Montpellier, France, 1994.

Hauksson, E., Earthquakes, faulting, and stress in the Los Angeles basin, *J. Geotech. Eng.*, *95*, 15,365–15,394, 1990.

Huftile, G., and R. Yeats, Convergence rates across a displacement transfer zone in the western Transverse Ranges, Ventura basin, California, *J. Geophys. Res.*, *100*, 2043–2067, 1995.

Huftile, G., and R. Yeats, Deformation rates across the placerita (NorthridgeMw=6.7 aftershock zone) and Hopper Canyon segments of the western Transverse Ranges deformation belt, *Bull. Seismo. Soc. Am.*, *86*, S3–S18, 1996.

Jaeger, J., and N. Cook, *Fundamentals of Rock Mechanics*, Chapman and Hall, London, 1976.

Jean, M., and J. Moreau, Dynamics of elastic or rigid bodies with frictional contact: Numerical methods, *Méc., Modélisation Numér. Dyn. Matér.*, *124*, 43–57, 1991.

Jean, M., and G. Touzot, Implementation of unilateral contact and dry friction in computer codes dealing with large deformation problems, *J. Appl. Mech.*, *7*, 145–160, 1988.

Kirby, S., Rheology of the lithosphere, *Rev. Geophys.*, *21*, 1458–1487, 1983.

Larsen, S. C., D. C. Agnew, and B. H. Hager, Strain accumulation in the Santa Barbara channel: 1970-1988, *J. Geophys. Res.*, *98*, 2119–2133, 1993.

Leroy, Y., and M. Ortiz, Finite element analysis of strain localization in frictional materials, *Int. J. Numer. Anal. Methods Geomech.*, *13*, 53–74, 1989.

Luyendyk, B., A model for neogene crustal rotations, transtension, and transpression in southern California, *Geol. Soc. Am. Bull.*, *103*, 1528–1536, 1991.

Luyendyk, B., M. Kamerling, and R. Terres, Geometric model for neogene crustal rotations in southern California, *Geol. Soc. Am. Bull.*, *91*, 211–217, 1980.

Molnar, P., Final report to the SCEC for work performed during the period from september through december, 1991, *Tech. rep.*, Southern California Earthquake Center, 1992.

Nagtegaal, J., D. Parks, and J. Rice, On numerically accurate finite element solutions in the fully plastic range, *Comput. Methods Appl. Mech. Eng.*, *4*, 153–177, 1974.

Namson, J., and T. Davis, Structural transect of the western Transverse Ranges, California: Implications for lithospheric kinematics and seismic risk evaluation, *Geology*, *16*, 675–679, 1988.

Nicholson, C., C. Sorlien, T. Atwater, J. Crowell, and B. Luyendyk, Microplate capture, rotation of the western Transverse Ranges, and initiation of the San Andreas transform as a low-angle fault system, *Geology*, *22*, 491–495, 1994.

Ode, H., Faulting as a velocity discontinuity in plastic deformation, *Geol. Soc. Am. Mem.*, *79*, 293–373, 1960.

Okada, Y., Internal deformation due to shear and tensile faults in a half-space, *Bull. Seismo. Soc. Am.*, *82*, 1018–1040, 1992.

Ramberg, H., Selective buckling of composite layers with contrasted rheological properties: A theory for simultaneous formation of several orders of folds, *Tectonophysics*, *1*, 307–341, 1964.

Ramsay, J., and M. Huber, *Modern Structural Geology*, vol. 2, Academic Press, Oxford, 1987.

Rudnicki, J., and J. Rice, Conditions for the localization of deformation in pressure-sensitive materials, *J. Mech. Phys. Solids*, *23*, 371–394, 1975.

Savage, J., Dislocations in seismology, in *Dislocations in Solids*, edited by F. Nabarro, pp. 251–339, North-Holland Publishing Co., New York, 1980.

Shaw, J., and J. Suppe, *Earthquake Hazards of Active Blind-Thrust Faults Under the Central Los Angeles Basin, California*, vol. 101, North-Holland Publishing Co., New York, 1996.

Strehlau, J., and R. Meissner, Estimation of crustal viscosities and shear stresses from an extrapolation of experimental steady state flow data, in *Composition, Structure and Dynamics of the Lithosphere-Asthenosphere System*, edited by Fuchs and Froidevaux, vol. 16 of *Geodyn. Ser.*, pp. 69–87, AGU Monograph, Washington, D.C., 1987.

Thibaut, M., J. Gratier, M. Leger, and J. Morvan, An inverse method for determining three-dimensional fault geometry with thread criterion, application to strike-slip and thrust faults (Western Alps and California), *J. Struct. Geol.*, *18*, 1127–1138, 1996.

Yeats, R., Neogene acceleration of subsidence rates in southern California, *Geology*, *6*, 456–460, 1978.

Yeats, R., Large scale quaternary detachments in Ventura basin, southern California, *J. Geophys. Res.*, *88*, 569–583, 1983.

Yeats, R., Late Cenozoic structure of the Santa Suzana fault zone, *U.S. Geol. Surv. Prof. Pap. 1339*, 1987a.

Yeats, R., Changing tectonic styles in cenozoic basins of southern California, in *Cenozoic Basin Development of Coastal California*, edited by R. Ingersoll and E. W.G., vol. 6 of *Rubey Ser.*, pp. 284–298, Prentice-Hall, Englewood Cliffs, NJ, 1987b.

Yeats, R., and G. Huftile, The Oak Ridge fault system and the 1994 Northridge earthquake, *Nature*, *373*, 418–420, 1995.

Yeats, R., G. Huftile, and L. Stitt, Late cenozoic tectonics of the east Ventura basin, Transverse Ranges, California, *AAPG Bull.*, *78*, 1040–1074, 1994.

Yerkes, R. F., and W. H. K. Lee, Maps showing faults and fault activity and epicenters, focal depths and focal mechanisms for 1970-1975 earthquakes, western transverse ranges, california, *U.S. Geol. Surv. Misc. Field Stud. Map, MF-1032*, 1979.

J. Chéry, Laboratoire de Géophysique et Tectonique, CNRS, Université Montpellier II, 34095 Montpellier Cedex 05, France. (e-mail: jean@dstu.univ-montp2.fr)

F. Niño, Department of Geology and Geophysics, University of Edinburgh, Grant Institute, West Mains Road, Edinburgh EH9 3JW, Scotland, UK. (e-mail: nino@glg.ed.ac.uk)

J.-P. Gratier, Laboratoire de Géophysique Interne et Tectonophysique, Université Joseph Fourier, CNRS-Observatoire, BP 53X 38041, Grenoble, France. (e-mail: gratier@lgit.obs.ujf-grenoble.fr)

(received October 13, 1997;
revised August 27, 1998;
accepted September 7, 1998.)